General Trends for Bulk Diffusion in Ice and Surface Diffusion on Ice

Frank E. Livingston,[†,§] Jamison A. Smith,[†,||] and Steven M. George*[,†,‡]

Department of Chemistry and Biochemistry and Department of Chemical Engineering, University of Colorado, Boulder, Colorado 80309-0215

Received: December 6, 2001; In Final Form: April 3, 2002

Experimental measurements of bulk diffusion in ice and surface diffusion on ice were performed using laser resonant desorption (LRD) techniques. Bulk diffusion in ice was examined using ice sandwich structures and continuous source experiments together with LRD depth-profiling analysis. Surface diffusion was monitored using prepare−refill−probe LRD experiments. New experimental results were obtained for the bulk diffusion of NH_3 and CH_3OH. These species probably exist as hydrates in the ice. The LRD measurements for CH_3OH hydrate diffusion, combined with previous results, provide evidence for a vacancy-mediated diffusion mechanism. The diffusion rates for NH_3 hydrates are much larger than diffusion rates for H_2O self-diffusion in ice and are attributed to the disruption of the ice lattice. LRD prepare−refill−probe experiments revealed that surface diffusion was not measurable for almost all of the species examined on ice. Only butane displayed a measurable surface mobility that was attributed to its unique size and chemical nature. These new measurements of bulk diffusion in ice and surface diffusion on ice should be useful in developing our understanding of kinetic processes in and on ice that are relevant to heterogeneous atmospheric chemistry and ice core analysis.

I. Introduction

Water ice is the most prevalent molecular solid in the atmosphere and on the surface of Earth. H_2O ice particles influence heterogeneous atmospheric chemistry in the polar stratosphere that leads to ozone depletion.[1,2] Glacial and polar ice contains an historic record of Earth's atmosphere that dates back over 400 000 years in some locations.[3−7] Ice also exists in many planetary, cometary, and interstellar media. Despite the importance of ice, very little is known about the kinetics of bulk diffusion in ice or surface diffusion on ice.

Fundamental diffusion measurements in ice or on ice are limited due to experimental challenges. Bulk diffusion measurements in ice have focused primarily on H_2O self-diffusion kinetics. Early diffusion studies used microtome sectioning and scintillation or mass spectrometric detection to measure the diffusion kinetics of isotopic probes ($H_2{}^{18}O$, D_2O, and T_2O) near the ice melting point.[8,9] Laser-induced thermal desorption (LITD) techniques have also been utilized to study HDO and $H_2{}^{18}O$ diffusion into pure[10−14] and HNO_3- and HCl-dosed[11,15] ice multilayers at lower temperatures of 140−180 K. The self-diffusion kinetics measured for the various isotopic tracers are similar and are consistent with a molecular transport mechanism.[8−10,12]

Limited studies exist regarding diffusion of other species in ice. The diffusion of several acids, including HCl,[16−23] HNO_3,[24−26] and HF,[27,28] has been examined using various techniques. For HCl diffusion, conflicting results have been reported with HCl diffusion coefficients ranging from $D \sim 10^{-5}$ cm^2/s to $D \sim 10^{-13}$ cm^2/s at $T = 185$ K.[16−23] The wide range of diffusion coefficients has been attributed to ice preparation conditions, varying species concentrations, variable defects and grain boundaries, and trapping phenomena.[16] Because of the variability of previous diffusion studies, the chemical and physical properties that control migration in ice are not well understood. An ongoing debate still exists over the mechanism of H_2O isotopic diffusion in ice.[8,9]

Surface diffusion measurements on ice are virtually nonexistent. Studies of H_2O surface migration on ice have been attempted using groove relaxation and interference microscopy.[29] These studies have investigated H_2O mass transfer on the basal (0001) facet of ice single crystals at $T = 263$ K. Unfortunately, complications involving evaporation−condensation and two-dimensional viscous flow prevented measurements of H_2O surface migration. Scanning LITD has also been utilized to study HDO and $H_2{}^{18}O$ surface diffusion on the basal plane of hexagonal pure[10,13,14] and acid-dosed[15] single-crystal ice multilayers on Ru(0001). Negligible surface migration allowed these LITD results to set an upper limit of $D_s \leq 1 \times 10^{-9}$ cm^2/s on the HDO and $H_2{}^{18}O$ surface diffusion coefficients at $T = 140$ K. The surface diffusion of H_2O on ice has also been investigated using theoretical methods.[30] The calculated diffusivity of 1×10^{-9} cm^2/s was the same as the experimental upper limit.

To better understand diffusion in ice, a new infrared laser resonant desorption (LRD) technique has been developed to depth profile into ice films and measure diffusion rates in ice.[16,31−35] LRD depth-profile analysis has been used to measure the diffusion of HCl hydrates[16,31] and sodium (Na)[31,32] in ice. In addition, the anion−cation trapping effects of Na on HCl hydrate diffusion[33] and HCl on Na diffusion[32] in ice have been examined using LRD probing. More recent LRD studies have explored the diffusion of formic acid (HCOOH) and acetic acid

* Corresponding author. Fax: (303) 492-5894. E-mail: Steven.George@Colorado.edu.
† Department of Chemistry and Biochemistry.
‡ Department of Chemical Engineering.
§ Current address: The Aerospace Corporation, Center for Microtechnology, 2350 E. El Segundo Blvd., El Segundo, CA 90245.
|| Current address: Laboratory for Atmospheric & Space Physics, University of Colorado, Boulder, CO 80309.

10.1021/jp014438c CCC: $22.00
Published on Web 06/11/2002

(CH_3COOH) in ice.[34] The results of these LRD examinations have raised many questions concerning the interplay between diffusion in ice and various molecular properties such as solubility, acidity and basicity, and size and geometry.

The present study explores the bulk and surface diffusion kinetics of a wide variety of molecules including a base (ammonia, NH_3), an alcohol (methanol, CH_3OH), a gaseous oxide (sulfur dioxide, SO_2), an alkane (butane, C_4H_{10}), a ketone (acetone, CH_3COCH_3), and an aromatic ring compound (benzene, C_6H_6). These measurements complement our earlier studies of acids (hydrogen chloride, HCl; formic acid, HCOOH; and acetic acid, CH_3COOH) and cations (sodium, Na). Bulk diffusion measurements were conducted using infrared LRD depth profiling on ice sandwich structures[16,31] and under continuous source conditions.[31,32] Surface diffusion measurements were performed using a new LRD prepare−refill−probe technique. These diffusion measurements expand upon our previous knowledge and allow us to begin to establish general trends concerning diffusion in the interior of ice and on the surface of ice.

II. Experimental Section

A. Vacuum Apparatus and Laser Resonant Desorption Technique. Earlier publications provided a detailed description of the experimental setup[16,31] and rotary Q-switched Er:YAG laser.[31,36] In brief, the LRD experiments were conducted in an ultrahigh vacuum (UHV) chamber located on a vibrationally isolated optical table. Crystalline ice films were grown on a single-crystal Ru(001) metal substrate. The excellent lattice match between Ru(001) and hexagonal ice promotes the growth of crystalline ice films.[14]

The measurements of diffusion in ice were performed using the infrared LRD depth-profiling technique.[16,31] LRD was accomplished using a Er:YAG TEM_{oo} Q-switched laser (Laser-Sight Technologies, Inc., Model 1-2-3) with an output wavelength of $\lambda = 2.94$ μm and a pulse duration of ~100 ns. A newly designed $BaSO_4$ diffuse reflector pump chamber (Shiva Laser Systems) was implemented to achieve high laser output energies and enhanced pulse-to-pulse stability.[31,36] The Er:YAG laser radiation resonantly pumps the O−H stretching vibration in the H_2O molecules in the ice lattice. The incident laser energy is rapidly thermalized and induces desorption in the near surface region of the ice film.[35]

In the LRD depth-profiling experiment, a series of Er:YAG laser pulses were used to desorb iteratively thin layer sections of the ice film.[16,31,35] The desorbed species were mass analyzed with high sensitivity using an Extrel C50 quadrupole mass spectrometer with line-of-sight to the ionizer. Consecutive laser pulses desorbed deeper into the ice bulk and measured the concentration profile of the diffusing species. The ice film thickness was determined using optical interferometry during isothermal desorption of the ice film following LRD depth-profile analysis.[37]

B. LRD Bulk Diffusion Measurements. One type of bulk diffusion measurement was performed by monitoring the concentration of the probe molecule in an ice sandwich versus time. This LRD depth-profiling method is illustrated in Figure 1 and has been described in detail in earlier publications.[16,31] Briefly, a laminated sandwich structure was prepared by initially growing an ice multilayer on the Ru(001) substrate. The bottom ice film was grown at temperatures in the range $T = 100-160$ K and subsequently annealed to ensure crystallinity. The probe molecule was then deposited on top of this ice multilayer. The ice laminate sandwich structure was completed by growing an additional ice layer on the probe molecule adlayer at $T = 120-140$ K.

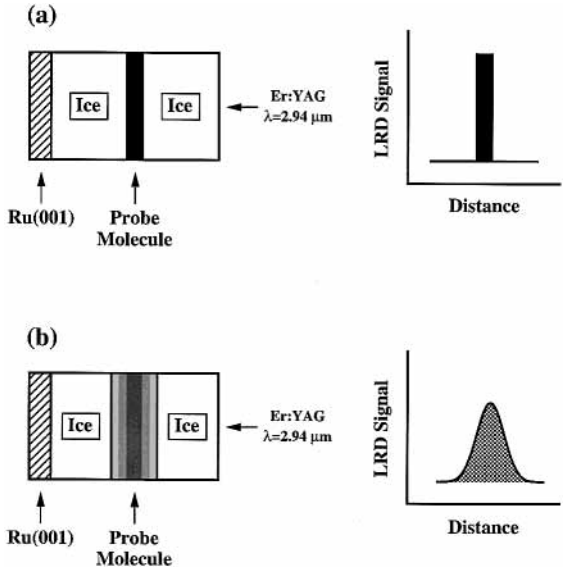

Figure 1. LRD depth-profiling experiment on an ice sandwich structure. (a) Er:YAG laser pulses depth profile the ice sandwich and measure the initial concentration gradient. (b) Second LRD depth profile observes the diffusional relaxation of the initial concentration gradient.

The Er:YAG laser was then used to depth profile into the ice laminate structure and measure the concentration profile of the probe molecule versus diffusion time. Prior to diffusion, the probe molecule should remain well localized in the ice sandwich and the initial LRD depth profile should resemble a top-hat profile as shown in Figure 1a. The temperature of the ice laminate was then raised to the desired diffusion temperature for a fixed time interval. After the diffusion of the probe molecule, the ice multilayer was cooled rapidly to terminate further diffusion and a second LRD depth profile was obtained using the Er:YAG laser. Diffusion of the interlayer species will result in the relaxation of the initial top-hat profile as illustrated in Figure 1b. The diffusion coefficients were extracted by modeling the diffusion process as the relaxation of an extended initial distribution in an infinite medium.[38]

A second type of bulk diffusion measurement was performed by monitoring the concentration of the probe molecule versus distance into the ice film. For this experiment, the ice film was continuously exposed to the probe molecule as depicted in Figure 2 and described in detail elsewhere.[31,32] In brief, an ice film was initially prepared by H_2O vapor deposition on the Ru(001) substrate. The H_2O ice film was then exposed continuously to the probe molecule for a fixed time duration. This exposure occurred at the desired diffusion temperature as depicted in Figure 2a. Following the constant exposure, the ice film was cooled to minimize any further diffusion. The Er:YAG laser was then used to probe sequentially into the ice film to measure the concentration profile as shown in Figure 2b. Diffusion coefficients were derived by modeling the concentration profile as diffusion in a semi-infinite medium under continuous source conditions.[38]

C. LRD Surface Diffusion Measurements. In the surface diffusion experiment, a single Er:YAG laser pulse is used to desorb the probe molecules from the ice film surface as shown in Figure 3a. Laser pulses were incident onto the ice film at an angle of 54° with respect to the surface normal. Using a 760 mm focal length lens, this optical geometry produced elliptical

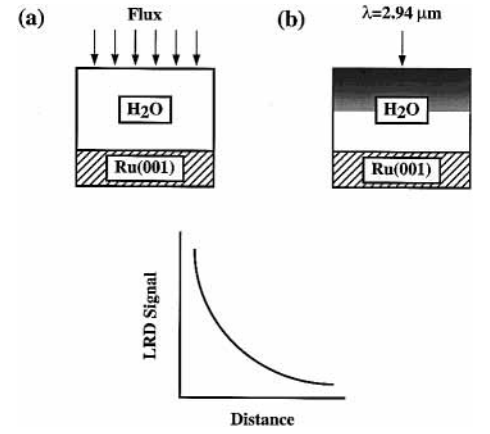

Figure 2. Continuous source LRD depth-profiling experiment. (a) Ice film is exposed to a continuous flux for a fixed time at constant temperature. (b) Er:YAG laser pulses depth profile the ice film and measure the concentration gradient.

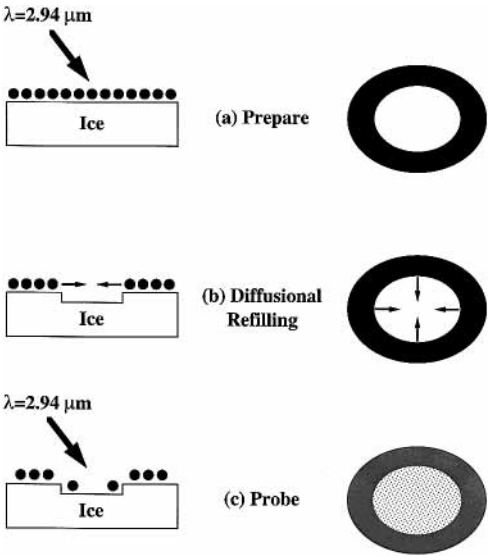

Figure 3. Prepare−refill−probe LRD surface diffusion experiment. (a) Er:YAG laser prepare pulse creates an evacuated region by desorbing the adsorbates from the ice surface. (b) Surrounding adsorbates diffuse into the initially evacuated region. (c) Second Er:YAG laser probe pulse measures the diffusional refilling.

desorption areas with typical dimensions of ~175 μm × ~225 μm as measured by spatial autocorrelation methods.[39] The laser beam was translated across the ice film using mirrors mounted on piezoelectric translators. A typical H_2O desorption depth during LRD was ~0.5 μm using pulse energies of ~0.6 mJ. The LRD regions were separated by 750 μm.

The probe molecules then may diffuse into the evacuated LRD region as depicted in Figure 3b. After a time delay, a second identical Er:YAG laser pulse heats the same area as shown in Figure 3c. The second laser pulse desorbs the probe molecules that have refilled the initially evacuated LRD region. The LRD signal at each delay time corresponds to the amount of diffusional refilling. The surface diffusion coefficients were calculated by fitting the time-dependent LRD refilling signals using Fick's second law and accounting for the elliptical geometry of the LRD region.[40−42]

D. Preparation of Ice Multilayers and Deposition of Diffusion Species. Ice multilayers were grown by vapor deposition of $H_2{}^{16}O$ on the Ru(001) substrate using a capillary array doser. The high purity $H_2{}^{16}O$ (optima grade, Fisher Scientific) was purified by several freeze−pump−thaw cycles with liquid nitrogen prior to use. Deposition of the diffusion species was performed using a separate capillary array doser. Low temperatures (T = 105−120 K) were employed for deposition to avoid possible desorption or preliminary diffusion. The concentrations or coverages of the diffusion species were derived from cross-calibration with the measured H_2O LRD signals at m/e = 18 (H_2O^+) and temperature programmed desorption (TPD) analysis.

High purity gaseous samples of the diffusion species were obtained directly from the supplier and used without further purification. The gaseous samples included ammonia (NH_3, >99% anhydrous grade, Matheson Gas Products, Inc.), butane (C_4H_{10}, UHP grade, Matheson Gas Products, Inc.), and hydrogen chloride (HCl, >99% anhydrous grade, Aldrich Chemical Co., Inc.). Additional gaseous samples were sulfur dioxide (SO_2, >99.98% anhydrous grade, Matheson Gas Products, Inc.) and sulfur hexafluoride (SF_6, >99.8%, Scott Specialty Gases, Inc.).

The liquid samples were purified by repeated freeze−pump−thaw cycles with liquid nitrogen. The liquid samples included acetic acid (glacial CH_3COOH, assay 100.0%, Mallinckrodt), acetone (CD_3COCD_3, 99.9% D, Cambridge Isotope Laboratories, Inc.), benzene (C_6D_6, 99.6% D, Cambridge Isotope Laboratories, Inc.), and chloroform ($CDCl_3$, 99.8% D, Cambridge Isotope Laboratories, Inc.). Additional liquid samples were formic acid (86% HCOOH, assay 95.2%, Mallinckrodt), methanol (CH_3OH, >99.9% spectroanalyzed grade, Fisher Scientific), and water ($H_2{}^{18}O$, 95−98%, Cambridge Isotope Laboratories, Inc.). 1,1,1,2-Tetrafluoroethane (CF_3CH_2F) was extracted from EnviroTech Duster 1671 (Tech Spray, Inc.) by condensing the commercial gas phase product using liquid nitrogen and CO_2/acetone cooling baths.

III. Results

A. Bulk Diffusion in Ice. *1. Ammonia (NH_3).* NH_3 bulk diffusion in ice was measured using an ice sandwich structure. The thickness of the top and bottom ice layers was ~10 μm. The initial NH_3 interlayer coverage was ~1 × 10^8 NH_3 molecules/μm^2. Although this NH_3 coverage exceeds one NH_3 monolayer, the NH_3 can easily insert into the ice lattice.[43−45] The measured NH_3 LRD signals in the ice laminate structure are shown in Figure 4. The NH_3 was detected by monitoring NH^+ at m/e = 15. Each data point represents the NH_3 LRD signal derived from a single laser pulse and corresponds to an H_2O desorption depth during LRD of 0.57 μm at a laser pulse energy of E = 0.68 ± 0.05 mJ.

The LRD depth-profiling results in Figure 4a show that the NH_3 interlayer in the ice sandwich structure at 110 K is initially well localized at t = 0. The NH_3 interlayer width is less than the H_2O desorption depth, and all the NH_3 is desorbed in a single laser pulse. The temperature of the ice multilayer was then raised to T = 140.1 K for t = 120 s. Subsequently, the ice multilayer was cooled rapidly to ~110 K to terminate further NH_3 diffusion. The LRD results obtained after 120 s at 140.1 K are shown in Figure 4b.

Figure 4b reveals that the NH_3 coverage gradient has relaxed with NH_3 diffusion occurring over ~7−8 μm. The calibrated NH_3 LRD signal near the center of the NH_3 concentration profile in Figure 4b corresponds to ~8 × 10^7 NH_3 molecules/μm^3 or ~2.5 × 10^{-3} NH_3 mole fraction. Although the NH_3 equilibrium solubility in ice has not been reported, this NH_3 concentration probably exceeds the NH_3 impurity solubility limit in crystalline ice and corresponds to an NH_3 hydrate.[43,44] Simulations of the diffusion shown by the solid line in Figure 4b yield a NH_3 diffusion coefficient of D = 4.3 (±1.3) × 10^{-10} cm^2/s at T = 140.1 K.

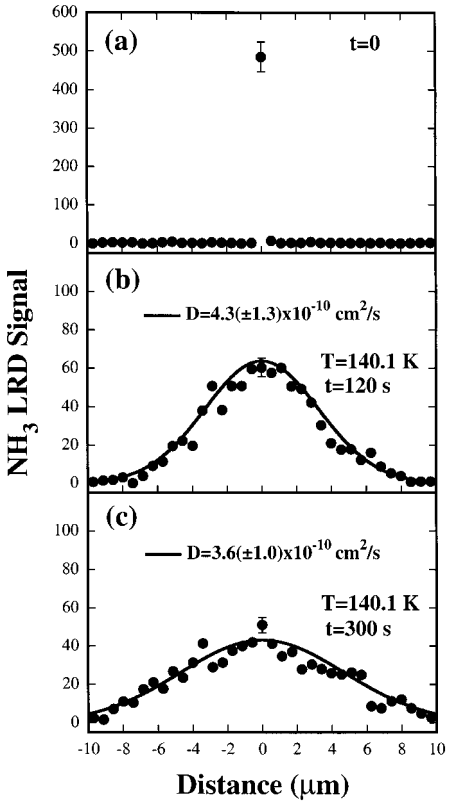

Figure 4. NH_3 concentration profiles measured using LRD depth profiling in ice/NH_3/ice sandwich structures (a) at $t = 0$, (b) after diffusion at $T = 140.1$ K for $t = 120$ s, and (c) after diffusion at $T = 140.1$ K for $t = 300$ s. Experimental LRD results are represented by the solid circles, and Fick's law diffusion simulations are shown as solid lines.

The LRD depth-profiling results obtained after a diffusion time of $t = 300$ s at $T = 140.1$ K are shown in Figure 4c. The NH_3 LRD results indicate that NH_3 migration has occurred over lengths of ~9−10 μm. The calibrated NH_3 LRD signal near the center of the NH_3 concentration profile in Figure 4c corresponds to NH_3 levels of $\sim 5 \times 10^7$ NH_3 molecules/μm^3 or $\sim 1.5 \times 10^{-3}$ NH_3 mole fraction. Diffusion simulations fit to the LRD data yield a NH_3 diffusion coefficient of $D = 3.6\ (\pm 1.0) \times 10^{-10}$ cm^2/s at 140.1 K. The NH_3 diffusion coefficients obtained after diffusion times of 120 and 300 s are within experimental error.

NH_3 diffusion can also be monitored by measuring the NH_3 concentration profile in ice after continuous NH_3 exposure at the diffusion temperature. NH_3 LRD diffusion results obtained after a continuous NH_3 exposure at 141.2 K are shown in Figure 5. The ice film was exposed to NH_3 at a partial pressure of $P = 1.2 \times 10^{-6}$ Torr for $t = 60$ s at 141.2 K. The thickness of the ice film was ~8 μm. The incident laser pulse energy was $E = 0.72 \pm 0.06$ mJ and corresponds to an H_2O desorption depth during LRD of 0.62 μm for each consecutive laser pulse.

The experimental LRD results for NH_3 and H_2O in Figure 5 are denoted by solid circles and open squares, respectively. Each data point represents the NH_3 and H_2O LRD signals derived from a single laser pulse. The LRD depth-profiling results reveal that NH_3 has diffused over distances of ~5−5.5 μm into the ice film during the 60 s NH_3 exposure at 141.2 K. The NH_3 concentration measured by the first laser pulse after this continuous source experiment was $\sim 8 \times 10^7$ NH_3 molecules/μm^3 or $\sim 2.5 \times 10^{-3}$ NH_3 mole fraction. This NH_3 concentration probably corresponds to an NH_3 hydrate.[43,44] The Fick's law simulation yielding the solid line was derived using a NH_3 diffusion coefficient of $D = 4.5\ (\pm 1.7) \times 10^{-10}$ cm^2/s at $T = 141.2$ K.

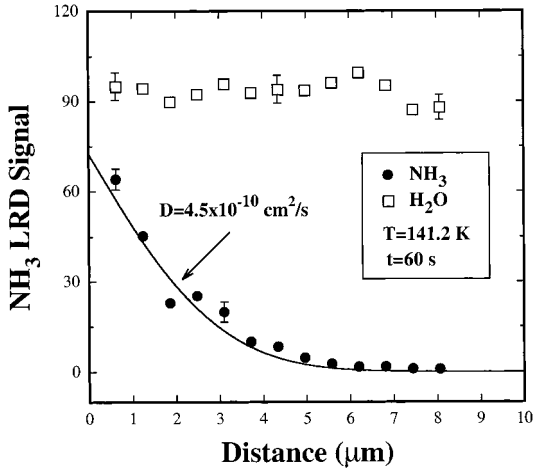

Figure 5. NH_3 and H_2O concentration profiles measured using LRD depth profiling following a continuous NH_3 exposure of $P = 1.2 \times 10^{-6}$ Torr for $t = 60$ s at a diffusion temperature of 141.2 K. Diffusion simulation shown by the solid line yields a diffusion coefficient of $D = 4.5 \times 10^{-10}$ cm^2/s.

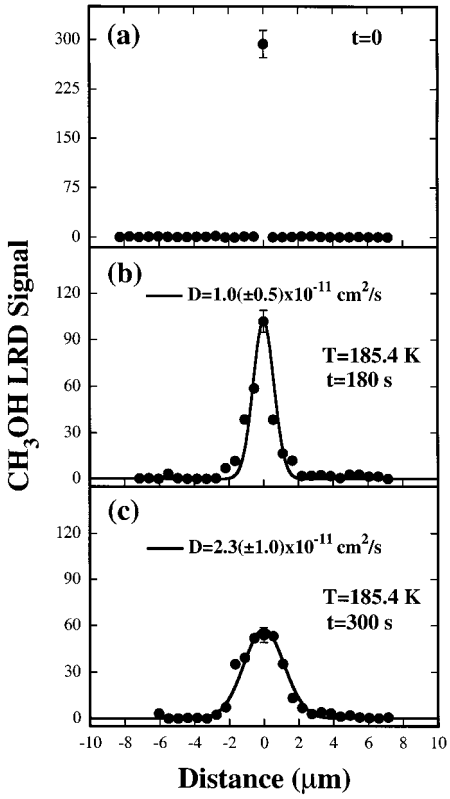

Figure 6. CH_3OH concentration profiles measured using LRD depth profiling in ice/CH_3OH/ice sandwich structures (a) at $t = 0$, (b) after diffusion at $T = 185.4$ K for $t = 180$ s, and (c) after diffusion at $T = 185.4$ K for $t = 300$ s. Experimental LRD results are represented by the solid circles, and Fick's law diffusion simulations are shown as solid lines.

2. Methanol (CH_3OH). Figure 6 shows the results for methanol diffusion in an ice sandwich structure. The thicknesses of the top and bottom ice layers were ~8 and ~7 μm, respectively. The initial CH_3OH interlayer coverage was $\sim 1 \times 10^8$ CH_3OH molecules/μm^2. The methanol was detected by monitoring CH_3O^+ at $m/e = 31$. The incident laser pulse energy

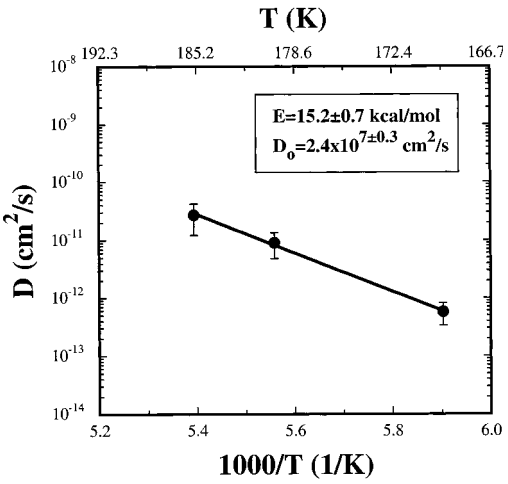

Figure 7. Arrhenius plot for temperature-dependent methanol (CH_3OH) bulk diffusion coefficients in ice measured using the LRD depth-profiling technique.

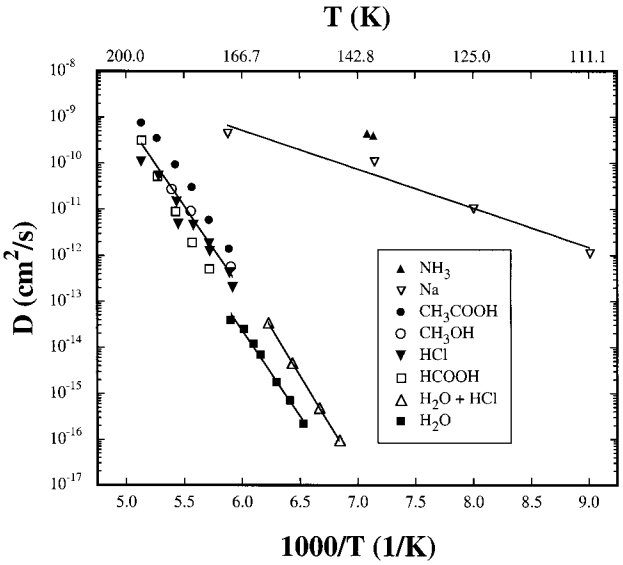

Figure 8. Arrhenius plots for temperature-dependent bulk diffusion coefficients of various species in ice measured using the LRD depth-profiling technique. H_2O bulk diffusion coefficients in pure and HCl-dosed ice were obtained using LITD methods.

was $E = 0.66 \pm 0.05$ mJ and corresponds to an H_2O desorption depth during LRD of ~ 0.55 μm for each laser pulse.

The LRD depth-profiling results obtained prior to CH_3OH diffusion at $t = 0$ are displayed in Figure 6a. These LRD results show that the CH_3OH interlayer remains well localized at $t = 0$ and $T = 110$ K. The temperature of the ice sandwich structure was then raised to $T = 185.4$ K for $t = 180$ s. Subsequently, the ice film was cooled rapidly to ~ 110 K to prevent further CH_3OH diffusion. The CH_3OH LRD coverage profile measured at $t = 180$ s is shown in Figure 6b.

Figure 6b reveals that the CH_3OH coverage gradient has relaxed with CH_3OH diffusion occurring over $\sim 1.5-2$ μm. The calibrated CH_3OH LRD signal near the center of the CH_3OH concentration profile in Figure 6b corresponds to CH_3OH levels of $\sim 1 \times 10^8$ CH_3OH molecules/μm^3 or $\sim 3 \times 10^{-3}$ CH_3OH mole fraction. Because no previous studies have established the CH_3OH impurity solubility limit in crystalline ice, these CH_3OH concentrations may correspond to CH_3OH hydrates.[46−50] The solid line corresponding to the solid circles in Figure 6b represents a fit to the CH_3OH LRD signals with $D = 1.0$ (± 0.5) $\times 10^{-11}$ cm^2/s.

The LRD depth-profiling results obtained after diffusion at $T = 185.4$ K for $t = 300$ s are shown in Figure 6c. These CH_3OH LRD results demonstrate that the CH_3OH coverage gradient has relaxed further with CH_3OH diffusion occurring over lengths of ~ 3 μm. The calibrated CH_3OH LRD signal near the center of the CH_3OH concentration profile in Figure 6c corresponds to CH_3OH levels of $\sim 6 \times 10^7$ CH_3OH molecules/μm^3 or $\sim 2 \times 10^{-3}$ CH_3OH mole fraction. Diffusion simulations yielded a CH_3OH diffusion coefficient of $D = 2.3$ (± 1.0) $\times 10^{-11}$ cm^2/s at $T = 185.4$ K.

The temperature dependence of the methanol diffusion was investigated over a small temperature range to extract the CH_3OH diffusion kinetic parameters. The Arrhenius data for CH_3OH diffusion in ice is shown in Figure 7. LRD depth-profiling measurements derived CH_3OH diffusion coefficients that ranged from $D = 5.7$ (± 0.6) $\times 10^{-13}$ cm^2/s at $T = 169.4$ K to $D = 2.7$ (± 1.3) $\times 10^{-11}$ cm^2/s at $T = 185.4$ K. Arrhenius analysis yielded a CH_3OH diffusion activation energy of $E_d = 15.2 \pm 0.7$ kcal/mol and a diffusion preexponential of $D_o = 2.4 \times 10^{7\pm0.3}$ cm^2/s.

3. Other Molecules. LRD depth-profiling analysis was also applied to study the bulk diffusion of sulfur dioxide (SO_2) in ice sandwich structures. Typical initial SO_2 interlayer coverages were $\sim 5 \times 10^8$ SO_2 molecules/μm^2. The diffusion times and diffusion temperatures were $T = 160.0-180.0$ K and $t = 10-30$ min, respectively. The sulfur dioxide was measured by monitoring SO_2^+ at $m/e = 64$. These LRD depth-profiling diffusion results indicated that SO_2 diffusion in the ice bulk was not detected under the experimental conditions. Only an upper limit of $D \leq 1.5 \times 10^{-12}$ cm^2/s can be derived for the SO_2 diffusion coefficient in ice using $\langle x^2 \rangle = 2Dt$.

Similar LRD depth-profiling experiments were conducted to investigate the diffusion of butane (C_4H_{10}) in ice. These LRD experiments utilized ice/C_4H_{10}/ice sandwich structures that contained initial C_4H_{10} interlayer coverages of $\sim 2 \times 10^8$ C_4H_{10} molecules/μm^2. The butane concentration profiles were measured by monitoring $C_3H_7^+$ at $m/e = 43$. The LRD depth-profiling results showed that the C_4H_{10} did not diffuse a distance that exceeded the H_2O desorption depth during LRD of ~ 0.5 μm. These LRD results imply a similar upper limit to the butane diffusion coefficient in ice of $D \leq 1.5 \times 10^{-12}$ cm^2/s.

The LRD bulk diffusion measurements for ammonia, methanol, sulfur dioxide, and butane complement our previous LRD studies of acid and alkali-metal diffusion in ice. LRD depth-profile analysis has been used recently to measure the diffusion kinetics of HCl hydrates[16,31] and sodium (Na)[31,32] in ice. More recent LRD studies have explored the diffusion of weak organic acids, such as formic acid (HCOOH) and acetic acid (CH_3COOH), in ice.[34] A comparison of the Arrhenius results for the diffusion of these species, together with the previous LITD results for H_2O isotope diffusion in ice,[10−12,15] is shown in Figure 8. The diffusion coefficients and diffusion kinetic parameters measured using LRD depth profiling are summarized in Table 1.

B. Surface Diffusion Results. *1. Survey of Various Molecules*. LRD surface diffusion experiments on ice were also conducted for a wide variety of molecules. These molecules included acetic acid (CH_3COOH), acetone (CD_3COCD_3), ammonia (NH_3), benzene (C_6D_6), chloroform ($CDCl_3$), formic acid (HCOOH), hydrogen chloride (HCl), methanol (CH_3OH), sulfur dioxide (SO_2), sulfur hexafluoride (SF_6), water ($H_2{}^{18}O$), and 1,1,1,2-tetrafluoroethane (CF_3CH_2F). Diffusional refilling was not observed for any of these molecules at temperatures and diffusion times of $T = 130.0-160.1$ K and $t \leq 3600$ s.

To measure surface migration on the ice film, the LRD

TABLE 1: Summary of Bulk Diffusion Kinetics in Ice Measured Using Infrared LRD Depth Profiling

diffusion species	D (cm^2/s)	diffusion T (K)	E_d (kcal/mol)	D_o (cm^2/s)	ref
HCl	2.0×10^{-13}−1.1×10^{-10}	169.0−194.9	15.3 ± 1.0	$1.5 \times 10^{7\pm0.2}$	16, 31
Na	1.1×10^{-12}−4.5×10^{-10}	111.0−170.3	3.9 ± 0.5	$6.2 \times 10^{5\pm0.3}$	31, 32
HCOOH	5.3×10^{-13}−3.2×10^{-10}	175.1−194.9	21.8 ± 0.9	$8.0 \times 10^{14\pm0.1}$	34
CH_3COOH	1.4×10^{-12}−7.6×10^{-10}	169.9−194.9	17.0 ± 0.7	$1.0 \times 10^{10\pm0.1}$	34
NH_3	4.0×10^{-10}	140.1			this study
	4.5×10^{-10}	141.2			this study
CH_3OH	5.7×10^{-13}−2.7×10^{-11}	169.4−185.4	15.2 ± 0.7	$2.4 \times 10^{7\pm0.3}$	this study
SO_2	$\leq 1.5 \times 10^{-12}$	160.0−180.0			this study
C_4H_{10}	$\leq 1.5 \times 10^{-12}$	160.0−180.0			this study

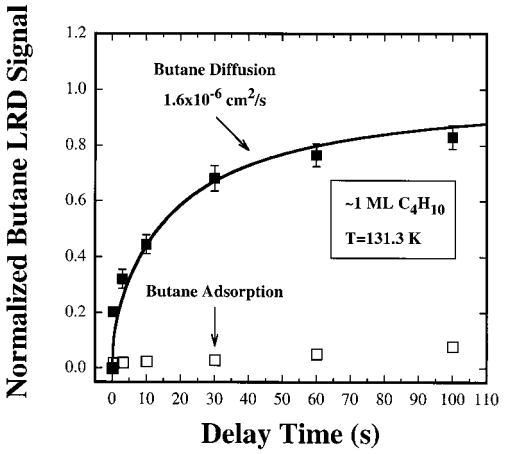

Figure 9. Butane diffusion refilling signals measured using the prepare−refill−probe LRD experiment at a diffusion temperature of $T = 131.3$ K. The solid line corresponds to a surface diffusion coefficient of $D = 1.6 \times 10^{-6}$ cm^2/s. Butane adsorption from the background has been subtracted from the butane diffusion refilling signal.

probing technique requires a ∼10% refilling of the initially evacuated laser desorption region. A ∼10% refilling of the elliptical desorption region with a major axis of ∼225 μm and a minor axis of ∼175 μm corresponds to a diffusion distance of ∼5 μm. Using $\langle x^2 \rangle = 2Dt$ and $t \leq 3600$ s, the LRD results imply an upper limit of $D \leq \sim 4 \times 10^{-11}$ cm^2/s for the surface diffusion coefficient of all the above molecules on ice.

2. Butane (C_4H_{10}). Butane surface diffusion on ice was also examined using the LRD prepare−refill−probe technique. Unlike the results for all the other molecules, surface diffusion was observed for butane. Typical normalized butane LRD refilling signals versus laser probe delay time are shown in Figure 9. This surface diffusion experiment was performed at $T = 131.3$ K. The butane surface coverage was $\sim 1 \times 10^7$ butane molecules/μm^2 or ∼1 monolayer (ML). The butane exposure conditions required to yield ∼1 ML of butane were determined using temperature programmed desorption (TPD) analysis. The integrated area of the TPD peak from this ∼1 ML butane coverage on ice was similar to the integrated area of the TPD peak from a saturated butane monolayer on Ru(001).[50] The underlying ice film thickness was ∼5 μm. The Er:YAG laser pulse energy was $E = 0.65 \pm 0.05$ mJ and corresponds to an H_2O desorption depth during LRD of 0.54 μm for each laser pulse.

Each data point in Figure 9 represents the LRD refilling signal derived from a single laser pulse. Butane was measured by monitoring $C_3H_7^+$ at $m/e = 43$. The measured butane LRD signal at each delay time was normalized using the initial butane LRD signals obtained during the preparation process. The LRD results for butane surface diffusion reveal that the initially evacuated region is nearly completely refilled after ∼100 s. The diffusional refilling data was analyzed using Fick's second law with an initial evacuated elliptical region with an aspect ratio of 1.3. Similar diffusion analysis has been performed in earlier LITD surface diffusion experiments.[40,51,52] The solid line in Figure 9 represents a best fit to the experimental LRD refilling data at $T = 131.3$ K. This fit was generated using a constant diffusion coefficient of $D = 2.0\ (\pm 1.0) \times 10^{-6}$ cm^2/s.

The impurity level of butane in the ice film was monitored prior to butane exposure. LRD probing revealed that the butane impurity levels in the ice films were typically ≤3% of a monolayer. Additional experiments were performed to check for background contributions to the measured butane LRD refilling signals. Following ice film growth, the ice film was exposed via backfilling to a butane pressure that was comparable to the background butane pressure during an LRD surface diffusion experiment. The normalized butane LRD signals derived from background adsorption are shown in Figure 9 and denoted by open squares. These LRD signals were normalized using the butane LRD signals obtained from ∼1 ML of butane on ice. The LRD refilling signals shown in Figure 9 have been corrected for butane background adsorption.

IV. Discussion

A. Bulk Diffusion Mechanism in Ice. Studies regarding the diffusion mechanism in ice are extremely scarce. The issue of whether the diffusion of H_2O and other impurtiy molecules (or atoms) in ice proceeds via a vacancy- or interstitial-mediated transport mechanism is currently unresolved.[53,54] Crystal lattice defects, such as interstitial (Frenkel) or vacancy (Schottky) defects, permit the diffusion of species through the crystal lattice. An atom or molecule may move from a normal lattice position into a neighboring vacancy or jump from interstitial site to interstitial site. X-ray topography experiments on the growth processes associated with dislocation loops and dipoles revealed that the predominant point defects in ice are self-interstitials at temperatures exceeding 223 K.[53,54] Consequently, H_2O self-diffusion is tentatively believed to occur by an interstitial-mediated mechanism for $T > 223$ K and by a vacancy-mediated mechanism for $T < 223$ K.[53,54]

Previous LRD experiments concerning HCl hydrate diffusion[16] in ice revealed that the HCl diffusion kinetics were very similar to the H_2O diffusion[10−13,15] kinetics in ice. The similarity between these diffusion kinetics is revealed in Figure 8. This correspondence argued for a vacancy-controlled diffusion mechanism for HCl hydrates in ice.[16] H_2O vacancies may be required to diffuse to lattice sites adjacent to H_3O^+ and Cl^- species in the hydrate prior to their migration into the vacancy sites. The diffusion of formic acid and acetic acid also display diffusion kinetics shown in Figure 8 that are nearly equivalent to the HCl diffusion kinetics.[33] This near equivalence argues for a similar diffusion mechanism.

In contrast, recent LRD experiments on Na diffusion[32] in ice showed that Na diffuses markedly faster than H_2O in ice. A comparison between H_2O isotope diffusion kinetics and Na

diffusion kinetics is shown in Figure 8. The H_2O diffusion coefficient in ice is $D = 1.2 \times 10^{-18}$ cm^2/s at $T = 140$ K.[10] The Na diffusion coefficient in ice at 140 K is $D = 5.1 \times 10^{-11}$ cm^2/s or $\sim 4 \times 10^7$ times larger compared with H_2O diffusion in ice.[32] This vast difference suggests either that Na^+ migrates rapidly through the interstitial hexagonal shafts of the ice lattice structure or that the Na^+ ions and their corresponding solvated electrons or hydroxyl ions (OH^-) significantly disrupt the ice lattice.[32]

B. Ammonia Bulk Diffusion in Ice. Figure 8 reveals that NH_3 diffuses extremely rapidly in ice. The NH_3 diffusion coefficients at $T = 140$ K are $\sim 3 \times 10^8$ times larger than the H_2O self-diffusion coefficient. This suggests that NH_3 hydrate diffusion is not mediated by H_2O vacancies in the ice lattice. The NH_3 LRD diffusion coefficients are very close to the Na diffusion coefficients.[32] In similarity to the proposed mechanisms for Na diffusion,[32] the NH_3 hydrate may disrupt the ice lattice. This disruption may prevent any comparison with vacancy- and interstitial-mediated diffusion in crystalline ice.

The NH_3 diffusion results can also be compared with previous investigations of NH_3 interaction with ice using transmission Fourier transform infrared (FTIR) spectroscopy.[43,44] The FTIR studies measured the conversion of ice nanocrystals with a $\sim$20 nm diameter to the mono- and hemihydrates (and deuterates) of ammonia at temperatures of $T = 100-128$ K.[43] The ammonia hydrate formation involves the diffusion of NH_3 through the ammonia hydrate crust that encompasses the ice particle.[43] The ice-to-ammonia hydrate conversion process is believed to be similar to the formation of HCl−ice hydrates.[55−57] One difference is that the conversion of D_2O ice nanocrystals to ammonia deuterates ($NH_3 \cdot D_2O$) occurs without significant isotopic H/D exchange.[44] These results argue for a molecular (NH_3) diffusion mechanism rather than an ionic mechanism involving ammonium (NH_4^+) and hydroxide (OH^-) ions.

The conversion rates of ice nanocrystals to the ammonia hemihydrates were used to derive the NH_3 diffusion rates.[43] For NH_3 diffusion within the amorphous hemideuterate, the NH_3 diffusion coefficients ranged from $D = 2.8 \times 10^{-19}$ cm^2/s at $T = 102$ K to $D = 9.4 \times 10^{-18}$ cm^2/s at $T = 107$ K.[43] Arrhenius analysis of the NH_3 diffusion rates within the amorphous hemideuterate yielded an NH_3 diffusion activation energy of $E_d = 15$ kcal/mol and a diffusion preexponential of $D_o = 7 \times 10^{13}$ cm^2/s. The NH_3 diffusion coefficients were larger in the crystalline hemideuterate and ranged from $D = 1.1 \times 10^{-17}$ cm^2/s at $T = 107$ K to $D = 1.4 \times 10^{-16}$ cm^2/s at $T = 112$ K.[43] Arrhenius analysis yielded an NH_3 diffusion activation energy of $E_d = 12$ kcal/mol and a diffusion preexponential of $D_o = 9 \times 10^7$ cm^2/s.

The FTIR results for NH_3 diffusion in ammonia hydrates are consistent with the NH_3 diffusion coefficients measured using LRD depth profiling. Extrapolation of the FTIR results for the NH_3 diffusion kinetics to the higher temperatures employed in the LRD diffusion experiments yields an NH_3 diffusion coefficient of $D \sim 3 \times 10^{-10}$ cm^2/s and $D \sim 2 \times 10^{-11}$ cm^2/s at $T = 140.1$ K for the amorphous and crystalline hemideuterates, respectively. These NH_3 diffusion coefficients are similar to the NH_3 diffusion coefficient of $D = 4.0 \times 10^{-10}$ cm^2/s at 140.1 K measured using LRD depth profiling.

Additional information on the interaction of NH_3 with ice is obtained using infrared reflection absorption spectroscopy (IRAS) and thermal desorption analysis.[58] NH_3 adsorption and solvation was examined on ultrathin ice films grown on a Ru(001) substrate. Initial NH_3 adsorption on the ice surface at $T = 38$ K occurred via hydrogen-bonding and HOH−NH_3 interactions rather than ionic bonding with HO^-−NH_4^+ interactions.[58] However, heating of the ice film to $T = 120$ K induced NH_3 ionization at the ice surface and subsequent transfer of NH_4^+ species into the ice bulk. A diffusion coefficient for NH_4^+ of $D \geq 5 \times 10^{-16}$ cm^2/s at $T = 120$ K was estimated from the IRAS results using the one-dimensional Einstein−Smoluchowski equation. This NH_4^+ diffusion coefficient falls within the range of the NH_3 diffusion coefficients measured using LRD depth profiling and FTIR spectroscopy.

C. Methanol Bulk Diffusion in Ice. Figure 8 shows that the CH_3OH diffusion kinetics in ice measured using LRD depth profiling are very similar to the HCl hydrate[16] and H_2O diffusion kinetics obtained previously.[10−13,15] This close agreement argues that methanol hydrate diffusion in ice occurs via a vacancy-mediated transport mechanism. H_2O vacancies in the ice may need to diffuse to lattice sites in the ice that are adjacent to species in the methanol hydrate. The methanol hydrate species can then move into the vacancies and diffuse in the ice.

Previous studies have reported the existence of both methanol clathrate hydrates[46−48] and methanol hydrates.[48−50] Amorphous co-deposits of water and methanol are observed to crystallize when heated to 130−140 K.[46] Their electron diffraction patterns are consistent with type II clathrate hydrates.[46] Far-infrared investigations also observe the crystallization of H_2O:CH_3OH = 2:1 mixtures after annealing to 140 K.[47] However, theoretical studies have questioned the stability of the methanol clathrate hydrate structure at any temperature.[49] These simulations suggest that the host network always partially breaks in order to form guest−host hydrogen bonds.[49] Infrared studies also indicate that the clathrate structures have limited stability and may form at low temperatures only because of kinetic factors.[48]

If the crystalline structures observed by the electron diffraction patterns are not methanol clathrate hydrates, they are most likely methanol hydrates. The diffraction patterns[46] and the sharp features observed in the far-infrared[47] must be associated with an ordered structure. Because the theoretical simulations predict CH_3OH-H_2O hydrogen bonding[49] and the far-infrared spectra suggest strong CH_3OH-H_2O interactions,[47] this ordered structure is probably a methanol hydrate. Methanol has been reported to form a crystalline monohydrate.[50] Unfortunately, these results are not in the published literature. Infrared studies are also consistent with the formation of lower hydrates as a result of annealing water and methanol co-deposits in a vacuum.[48]

The methanol hydrate is proposed to diffuse in the ice sandwich structure by undergoing progressive dilution. Methanol hydrate domains may move in the crystalline ice via H_2O vacancies. The methanol hydrate domain size may become progressively smaller as the methanol hydrate is diluted in the ice. Alternatively, the methanol hydrate may undergo a series of transformations during the dilution. This transformation may follow the progression monohydrate, dihydrate, trihydrate, and so on depending on the stability of these methanol hydrates.

D. SO_2 and Butane Bulk Diffusion in Ice. The diffusion of SO_2 and butane in ice was not measurable using the LRD depth-profiling techniques. Only an upper limit of $D \leq 1.5 \times 10^{-12}$ cm^2/s could be assigned from the ice sandwich structure experiments. Previous measurements of SO_2 incorporation into ice crystals imply a maximum SO_2 diffusion coefficient in ice of $D \leq 2 \times 10^{-10}$ cm^2/s at $T = 258$ K.[59] Recent experiments have also investigated SO_2 uptake into snow crystals at the ice melting point.[60] These depth-profile measurements suggest a much higher upper limit for the SO_2 diffusion coefficient of $D \leq 3 \times 10^{-4}$ cm^2/s. The LRD depth-profile results are

consistent with the estimates for SO_2 diffusion in ice at lower temperatures where the liquid-like layer is not present.

No previous measurements have been conducted that provide information on butane diffusion in ice. There have been studies of the adsorption isotherms for various *n*-alkanes on vapor-deposited ice over a temperature range of $T = 177-243$ K.[61] Unfortunately, adsorption isotherm results were not reported for *n*-butane. The adsorption isotherms for ethane (C_2H_6) and propane (C_3H_8) at $T = 177$ K and $T = 195$ K, respectively, display slow ethane and propane adsorption that was extremely high and irreversible to desorption.[61] These observations were correlated with the ability of small, low molecular weight hydrocarbons to either diffuse and dissolve in the ice lattice or to undergo transformation into a hydrate or clathrate.[61,62]

The adsorption isotherms for *n*-pentane (C_5H_{12}) and *n*-hexane (C_6H_{14}) were also measured at $T = 223-243$ K and displayed markedly different adsorption.[61] The adsorption equilibrium was attained rapidly, and the adsorption amount was much lower. The adsorption isotherms were also reversible to desorption. These results suggested that larger chain hydrocarbons only equilibrate with the ice surface and do not diffuse into the ice lattice. Since *n*-butane does not show measurable diffusion in ice in the LRD depth-profiling experiments, *n*-butane should probably be grouped with the larger chain hydrocarbons that do not diffuse into the ice lattice.

E. General Trends for Bulk Diffusion in Ice. The results for NH_3 and CH_3OH hydrate diffusion from the present study, together with earlier LRD depth-profiling results, suggest some general trends for bulk diffusion in ice. These results are all displayed in Figure 8. Many of the molecules that display measurable bulk diffusion have diffusion kinetics that are nearly equivalent. The solid line through the data points for methanol, acetic acid, formic acid, and HCl hydrate diffusion represents a diffusion activation barrier of $E_d = 16.8 \pm 1.5$ kcal/mol and a diffusion preexponential of $D_o = 1.7 \times 10^{9\pm0.4}$ cm^2/s.

Figure 8 shows that the diffusion kinetics for these molecules are very similar to the diffusion kinetics for HDO diffusion in pure ice[10-12] and HCl-dosed ice.[11,15] HDO diffusion in pure ice displayed kinetics of $E_d = 17.0 \pm 1.0$ kcal/mol and $D_o = 4.2 \times 10^{8\pm0.08}$ cm^2/s. HDO diffusion in HCl-dosed ice yielded kinetics of $E_d = 19.0 \pm 0.3$ kcal/mol and $D_o = 2.4 \times 10^{12\pm0.02}$ cm^2/s. The similar diffusion kinetics for HDO and the other species argues strongly that a vacancy-mediated diffusion mechanism is responsible for the hydrate bulk migration. H_2O vacancies may be needed to diffuse to lattice sites adjacent to the hydrate prior to the diffusion of the hydrate species into the vacancy sites.

A vacancy-mediated mechanism has been proposed earlier for H_2O diffusion in ice at $T < 223$ K.[53,54] Based on the similar kinetics for H_2O diffusion and the diffusion of HCl hydrates, a vacancy-mediated mechanism was also proposed for HCl hydrate diffusion.[16] The results for methanol provided by this study, together with additional results for formic and acetic acid from other investigations,[34] add considerably to the preponderance of results displaying the same diffusion kinetics. These results argue that hydrates that do not significantly disrupt the ice lattice will display diffusion kinetics that are rate-limited by H_2O vacancy migration in ice.

Figure 8 also displays diffusional results that do not correspond to the diffusion kinetics of H_2O in ice. The diffusion coefficients for NH_3 provided by this study, as well as diffusion coefficients for Na obtained in earlier investigations,[32] are significantly larger than H_2O diffusion coefficients in ice. Diffusion coefficients larger than the H_2O self-diffusion coefficients could be explained by interstitial diffusion or by a severe disruption of the ice lattice. Interstitial diffusion of small molecules or ions in ice is possible in the large hexagonal shafts of crystalline ice that have diameters of ~3.8 Å.[63] NH_3 hydrates will define a new local crystalline environment that is significantly different than the ice lattice. However, the rapid NH_3 transport in ammonia hydrates has been correlated with the large channels in the exceptionally open structure of the ammonia hydrate lattice.[43]

F. Surface Diffusion on Ice. Most of the molecules investigated did not display measurable surface diffusion on ice. This lack of surface mobility can be attributed to absorption into the ice bulk. For polar molecules or molecules that dissociate, absorption into the ice bulk is favored for optimum solvation. Once the molecule is absorbed into the bulk, diffusion rates will be dictated by bulk diffusion rather than surface diffusion. Since bulk diffusion rates are expected to be much lower than surface diffusion rates, the upper limit for the surface diffusion coefficient of $D \leq 4 \times 10^{-11}$ cm^2/s determined by the LRD results is very reasonable.

For the molecules that do not interact strongly with ice, the lack of surface mobility may be attributed to island formation on the ice surface. If the molecule interacts more strongly with itself than with the ice surface, the molecules would be expected to form islands. Surface mobility would then either require the islands to move or individual molecules to break away and move as isolated molecules on the ice surface. Unfortunately, the molecules may also desorb if they have sufficient energy. Consequently, desorption may be observed prior to significant surface diffusion. This explanation was proposed earlier to explain the lack of measurable surface diffusion for NH_3 and CO_2 on Mg(100).[64,65]

Butane was the only molecule to display surface diffusion on ice. These LRD measurements of butane surface diffusion represent the first direct experimental observation of surface diffusion on ice. Earlier experimental studies measured the surface diffusion of butane on Ru(001).[66] The LRD surface diffusion results in Figure 9 reveal that butane migrates rapidly across the ice surface with a diffusion coefficient of $D = 1.6 (\pm0.5) \times 10^{-6}$ cm^2/s at $T = 131.3$ K. Additional measurements at temperatures from 129.9 to 131.9 K yielded diffusion coefficients of $D = 1.0 (\pm0.9) \times 10^{-6}-3.2 (\pm1.0) \times 10^{-6}$ cm^2/s. Because butane thermally desorbs from ice at temperatures from 135 to 150 K, temperatures of ~130 K allowed the surface diffusion to be measured with negligible thermal desorption.

Because all of the other molecules displayed no measurable surface diffusion, the surface diffusion experiment for butane was performed repeatedly to confirm the surface mobility. Numerous separate experiments amounting to 24 individual refilling curves were performed at temperatures of ~130 K to obtain the surface diffusion coefficients. Control experiments also revealed that butane adsorption onto the ice surface accounted for a small fraction (≤8%) of the measured refilling signal. This small amount of butane adsorption is shown in Figure 9 and was subtracted from the measured refilling LRD signal to yield the butane diffusion LRD signal shown in Figure 9.

The ability of butane to display measurable surface mobility may be attributed to its unique size and chemical nature. Smaller alkanes, such as ethane and propane, may diffuse down the hexagonal shafts into the ice bulk. Larger alkanes, such as pentane and hexane, may be restricted from diffusion into the hexagonal shafts because of their size. These alkanes are expected to remain at the ice surface because they are

hydrophobic, nonpolar, and highly insoluble in water. However, these larger molecules may also have larger adsorbate−adsorbate interactions that lead to island formation and limit diffusion. Butane may be unique because butane is too large to be adsorbed into the hexagonal shafts of ice, but small enough to minimize adsorbate−adsorbate interactions. Additional surface diffusion studies on longer chain alkanes are necessary to verify these proposals.

V. Conclusions

Laser resonant desorption (LRD) techniques were utilized to study bulk diffusion in ice and surface diffusion on ice. Measurements for a variety of molecules suggest a number of general trends for bulk diffusion in ice and surface diffusion on ice. On the basis of bulk diffusion LRD measurements for ammonia and methanol, together with previous LRD measurements for HCl, acetic acid, formic acid, and Na, there are two categories for bulk diffusion. CH_3OH, CH_3COOH, HCOOH, and HCl hydrates all display diffusion kinetics similar to the kinetics for H_2O self-diffusion in ice. This similarity argues that the diffusion of these hydrates is dependent on a vacancy-mediated diffusion mechanism. H_2O vacancies may be required to diffuse to lattice sites adjacent to the hydrate prior to the diffusion of hydrate species into the vacancy sites. In contrast, Na and NH_3 hydrates display diffusion kinetics much larger than for H_2O self-diffusion. This behavior argues for the disruption of the ice lattice.

Almost all the molecules displayed negligible surface diffusion on ice. This behavior was attributed to either absorption into the ice bulk or island formation on the ice surface that impedes surface diffusion. Only butane displayed measurable surface diffusion. Butane may be a special case because of its size and chemical nature. Butane may be too large to diffuse down the hexagonal shafts into the ice bulk. Butane is also nonpolar and unable to interact strongly with the polar ice surface. However, butane is also small enough to not interact strongly with itself and form islands that may have significantly reduced the surface diffusion. These general trends for bulk diffusion in ice and surface diffusion on ice should help our understanding of kinetic processes that affect heterogeneous atmospheric chemistry and ice core analysis.

Acknowledgment. The authors gratefully acknowledge the financial support of the National Science Foundation under Grant CHE-9905812. The authors also thank Dr. Roberto Bianco for his assistance with the computer simulations of butane surface diffusion on ice.

References and Notes

(1) Tabazadeh, A.; Turco, R. P. *J. Geophys. Res.* **1993**, *98*, 12727.
(2) Solomon, S. *Rev. Geophys.* **1988**, *26*, 131.
(3) Wolff, E. W.; Bales, R. C. *Chemical Exchange Between the Atmosphere and Polar Snow*; Springer-Verlag: Berlin, 1996.
(4) Mayewski, P. A.; Lyons, W. B.; Spencer, M. J.; Twickler, M. S.; Buck, C. F.; Whitlow, S. *Nature* **1990**, *346*, 554.
(5) Taylor, K. C.; Lamorey, G. W.; Doyle, G. A.; Alley, R. B.; Grootes, P. M.; Mayewski, P. A.; White, J. W.; Barlow, L. K. *Nature* **1993**, *361*, 432.
(6) Delmas, R. J.; Legrand, M. Long-Term Changes in the Concentrations of Major Chemical Compounds (Soluble and Insoluble) Along Deep Ice Cores. In *The Environmental Record in Glaciers and Ice Sheets Dahlem Workshop Report*; Oeschger, H., Langway, C. C., Eds.; Wiley and Sons: Chichester, UK, 1989.
(7) Petit, J. R.; Jouzel, J.; Raynaud, D.; Barkov, N. I.; Barnola, J.-M.; Basile, I.; Bender, M.; Chappellaz, J.; Davis, M.; Delaygue, G.; Delmotte, M.; Kotlyakov, V. M.; Kegrand, M.; Lipenkov, V. Y.; Lorius, C.; Pepin, L.; Ritz, C.; Saltzman, E.; Stievenard, M. *Nature* **1999**, *399*, 429.
(8) Petrenko, V. F.; Whitworth, R. W. *Physics of Ice*; Oxford University Press: New York, 1999.
(9) Hobbs, P. V. *Ice Physics*; Clarendon Press: Oxford, 1974.
(10) Livingston, F. E.; Whipple, G. C.; George, S. M. *J. Chem. Phys.* **1998**, *108*, 2197.
(11) Livingston, F. E.; George, S. M. *Defect Diffus. Forum* **1998**, *160*−*161*, 25.
(12) Livingston, F. E.; Whipple, G. C.; George, S. M. *J. Phys. Chem.* **1997**, *101*, 6127.
(13) George, S. M.; Livingston, F. E. *Surf. Rev. Lett.* **1997**, *4*, 771.
(14) Brown, D. E.; George, S. M. *J. Phys. Chem.* **1996**, *100*, 15460.
(15) Livingston, F. E.; George, S. M. *J. Phys. Chem. B* **1999**, *103*, 4366.
(16) Livingston, F. E.; George, S. M. *J. Phys. Chem. A* **2001**, *105*, 5155.
(17) Thibert, E.; Domine, F. *J. Phys. Chem. B* **1997**, *101*, 3554.
(18) Domine, F.; Thibert, E.; Silvente, E.; Legrand, M.; Jaffrezo, J.-L. *J. Atmos. Chem.* **1995**, *21*, 165.
(19) Horn, A. B.; Sully, J. *J. Chem. Soc., Faraday Trans.* **1997**, *93*, 2741.
(20) Wolff, E. W.; Mulvaney, R.; Oates, K. *Geophys. Res. Lett.* **1989**, *16*, 487.
(21) Krishnan, P. N.; Salomon, R. E. *J. Phys. Chem.* **1969**, *73*, 2680.
(22) Barnaal, D.; Slotfeldt-Ellingsen, D. *J. Phys. Chem.* **1983**, *87*, 4321.
(23) Molina, M. J.; Tso, T. L.; Molina, L. T.; Wang, F. C. Y. *Science* **1987**, *238*, 1253.
(24) Domine, F.; Thibert, E. *Geophys. Res. Lett.* **1996**, *23*, 3627.
(25) Domine, F.; Thibert, E. Relationship Between Atmospheric Composition and Snow Composition for HCl and HNO_3. In *Biogeochemistry of Seasonally Snow-Covered Catchments*; Tonnessen, K. A., Williams, M. W., Tranter, M., Eds.; Wallingsford: Oxfordshire, 1995.
(26) Sommerfeld, R. A.; Knight, C. A.; Laird, S. K. *Geophys. Res. Lett.* **1998**, *25*, 935.
(27) Haltenorth, H.; Klinger, J. *Solid State Commun.* **1977**, *21*, 533.
(28) Kopp, M.; Barnaal, D. E.; Lowe, I. J. *J. Chem. Phys.* **1965**, *43*, 2965.
(29) Itagaki, K. *J. Glaciol.* **1973**, *12*, 121.
(30) Batista, E. R.; Jonsson, H. *Comput. Mater. Sci.* **2001**, *20*, 325.
(31) Livingston, F. E.; Smith, J. A.; George, S. M. *Anal. Chem.* **2000**, *72*, 5590.
(32) Livingston, F. E.; George, S. M. Submitted for publication in *J. Phys. Chem. B* **2001**.
(33) Livingston, F. E.; George, S. M. *J. Phys. Chem. A* **2002**, in press.
(34) Livingston, F. E.; Bianco, R.; George, S. M. *J. Phys. Chem. B*, **2001**, in preparation.
(35) Krasnopoler, A.; George, S. M. *J. Phys. Chem. B* **1998**, *102*, 788.
(36) Livingston, F. E.; George, S. M.; Shori, R. K. *Rev. Sci. Instrum.* **2001**, in press.
(37) Haynes, D. R.; Tro, N. J.; George, S. M. *J. Phys. Chem.* **1992**, *96*, 8502.
(38) Crank, J. *The Mathematics of Diffusion*; Clarendon Press: Oxford, UK, 1975.
(39) George, S. M.; DeSantolo, A. M.; Hall, R. B. *Surf. Sci.* **1985**, *159*, L425.
(40) Mak, C. H.; Brand, J. L.; Deckert, A. A.; George, S. M. *J. Chem. Phys.* **1986**, *85*, 1676.
(41) Carslaw, H. S.; Jaeger, J. C. *Conduction of Heat in Solids*; Oxford University Press: Oxford, 1980.
(42) McLachlan, N. W. *Philos. Mag.* **1945**, *36*, 600.
(43) Uras, N.; Devlin, J. P. *J. Phys. Chem. A* **2000**, *104*, 5770.
(44) Delzeit, L.; Powell, K.; Uras, N.; Devlin, J. P. *J. Phys. Chem. B* **1997**, *101*, 2327.
(45) Uras, N.; Buch, V.; Devlin, J. P. *J. Phys. Chem. B* **2000**, *104*, 9203.
(46) Blake, D.; Allamandola, L.; Sandford, S.; Hudgins, D.; Freund, F. *Science* **1991**, *254*, 548.
(47) Hudson, R. L.; Moore, M. H. *Astrophys. J.* **1993**, *404*, L29.
(48) Williams, K. D.; Devlin, J. P. *J. Mol. Struct.* **1997**, *416*, 277.
(49) Koga, K.; Tanaka, H.; Nakanishi, K. *J. Chem. Phys.* **1994**, *101*, 3127.
(50) Tse, J. S.; Klug, D. D. *International Symposium on the Chemistry and Physics of Ice*; Hanover, NH, 1996.
(51) Brand, J. L.; Arena, M. V.; Deckert, A. A.; George, S. M. *J. Chem. Phys.* **1990**, *92*, 5136.
(52) Deckert, A. A.; Brand, J. L.; Arena, M. V.; George, S. M. *Surf. Sci.* **1989**, *208*, 441.
(53) Hondoh, T.; Goto, A.; Hoshi, R.; Ono, T.; Anzai, H.; Kawase, R.; Pimienta, P.; Mae, S. *Rev. Sci. Instrum.* **1989**, *60*, 2494.
(54) Goto, K.; Hondoh, T.; Higashi, A. *Jpn. J. Appl. Phys.* **1986**, *25*, 351.
(55) Devlin, J. P.; Uras, N.; Rahman, M.; Buch, V. *Isr. J. Chem.* **1999**, *39*, 261.
(56) Uras, N.; Rahman, M.; Devlin, J. P. *J. Phys. Chem. B* **1998**, *102*, 9375.
(57) Uras-Aytemiz, N., Joyce, C., Devlin, J. P. *J. Phys. Chem. A* **2001**, *105*, 10497.

(58) Ogasawara, H.; Horimoto, N.; Kawai, M. *J. Chem. Phys.* **2000**, *112*, 8229.
(59) Valdez, M. P.; Dawson, G. A. *J. Geophys. Res.* **1989**, *94*, 1095.
(60) Choi, J.; Conklin, M. H.; Bales, R. C.; Sommerfeld, R. A. *Atmos. Environ.* **2000**, *34*, 793.
(61) Orem, M. W.; Adamson, A. W. *J. Colloid Interface Sci.* **1969**, *31*, 278.
(62) Barrer, R.; Ruzika, D. *Trans. Faraday Soc.* **1962**, *58*, 2239.
(63) Eisenberg, D.; Kauzmann, W. *The Structure and Properties of Water*; Oxford University Press: New York, 1969.
(64) Arthur, D. A.; Meixner, D. L.; Boudart, M.; George, S. M. *J. Chem. Phys.* **1991**, *95*, 8521.
(65) Meixner, D. L.; Arthur, D. A.; George, S. M. *Surf. Sci.* **1992**, *261*, 141.
(66) Brand, J. L.; Deckert, A. A.; Arena, M. V.; George, S. M. *J. Chem. Phys.* **1990**, *92*, 5136.